




Article

Influence of the Incorporation of Basic or Amphoteric Oxides on the Performance of Cu-Based Catalysts Supported on Sepiolite in Furfural Hydrogenation

Antonio Guerrero-Torres ¹, Carmen P. Jiménez-Gómez ¹, Juan A. Cecilia ^{1,*} ,
Cristina García-Sancho ¹, José J. Quirante-Sánchez ² , Josefa M. Mérida-Robles ^{1,*}
and Pedro Maireles-Torres ¹ 

¹ Departamento de Química Inorgánica, Cristalografía y Mineralogía (Unidad Asociada al ICP-CSIC), Facultad de Ciencias, Campus de Teatinos, Universidad de Málaga, 29071 Málaga, Spain; guerrerotresantonio@gmail.com (A.G.-T.); carmenpig@uma.es (C.P.J.-G.); cristinags@uma.es (C.G.-S.); maireles@uma.es (P.M.-T.)

² Departamento de Química-Física, Facultad de Ciencias, Campus de Teatinos, Universidad de Málaga, 29071 Málaga, Spain; quirante@uma.es

* Correspondence: jacecilia@uma.es (J.A.C.); jmerida@uma.es (J.M.M.-R.);
Tel.: +34-952132373 (J.A.C.); +34-952132021 (J.M.M.-R.)

Received: 21 January 2019; Accepted: 19 March 2019; Published: 31 March 2019



Abstract: Cu-based catalysts supported on sepiolite have been tested in vapor-phase hydrogenation of furfural. The incorporation of basic or amphoteric metal oxides (magnesium oxide, zinc oxide, or cerium oxide) improves the catalytic behavior, reaching a maximum furfural conversion above 80% after 5 h of reaction at 210 °C. In all cases, the main product is furfuryl alcohol, obtaining 2-methylfuran in lower proportions. The incorporation of these metal oxide species ameliorates the dispersion of metallic Cu nanoparticles, increasing the number of available Cu⁰-sites, which enhances the catalytic performance. The presence of acid sites favors the hydrogenolysis of furfuryl alcohol towards 2-methylfuran, although it also causes an increase of carbon species on its surface, which is associated with the catalytic deactivation of the catalyst along the time-on-stream.

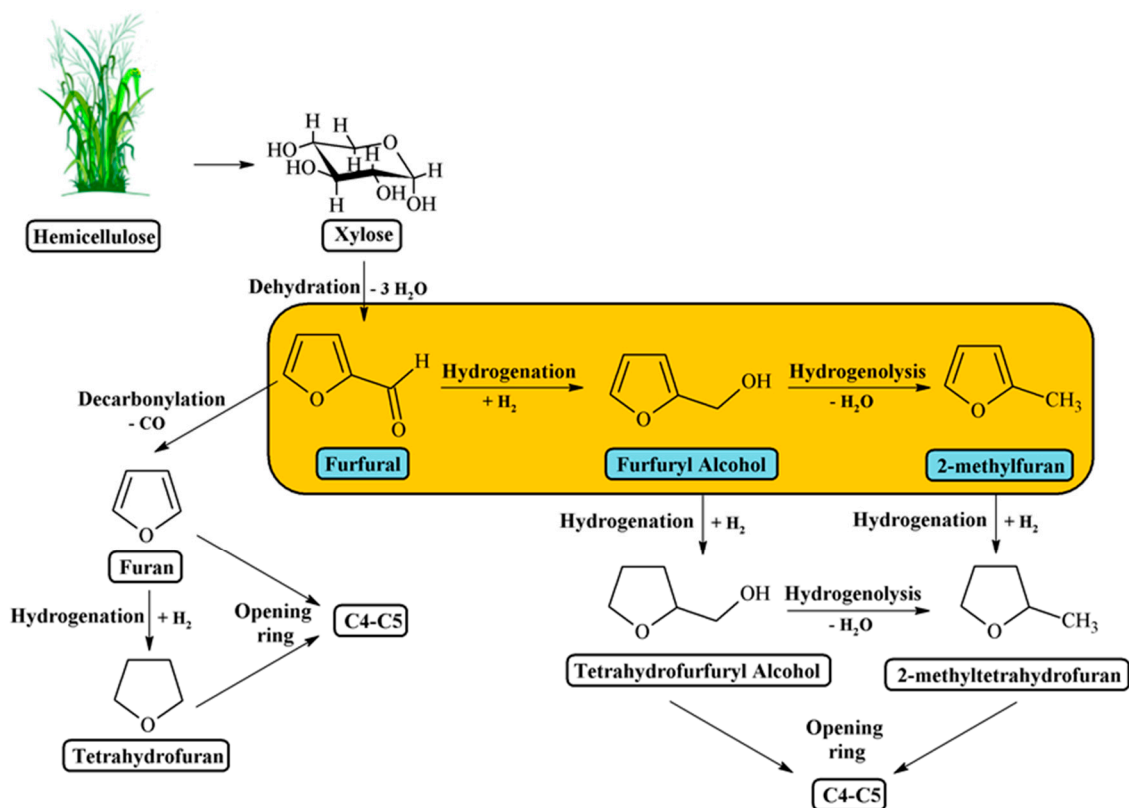
Keywords: Cu catalysts; metal oxide; supported sepiolite; furfural hydrogenation

1. Introduction

The future's society will require new technologies and processes for a sustainable production of chemicals and fuels. In this sense, biomass, and specifically lignocellulosic biomass, appears as a promising alternative to fossil fuels. On the other hand, a challenge for the development of the biorefinery, based on the use of biomass as feedstock, is the implementation of technologies to enhance the catalytic performance of existing processes. Thus, in the last years, these have improved the dehydration of pentoses and hexoses to produce furfural (FUR) and 5-hydroxymethylfurfural (HMF), respectively, increasing their potential as platform chemicals in biorefineries [1]. FUR has recently been considered as one of the key chemicals produced from lignocellulose, being a promising platform molecule for the synthesis of a wide variety of chemicals and biofuels [2–4].

Currently, there are several possible pathways to obtain valuable chemicals from FUR, and, among them, its selective hydrogenation to furfuryl alcohol (FOL) is the most important, since this is a relevant building block molecule for biofuels production and the manufacture of chemicals for resins, rubbers, and fibers [2–4]. FUR hydrogenation has been reported in vapor-phase using transition metals [2,4], liquid-phase using transition metals [5–7], and the catalytic transfer hydrogenation in liquid-phase in the presence of acid-base or metal sites [8–12].

Focusing on the FUR hydrogenation in vapor-phase, many efforts have been made in the search of more environmentally friendly catalysts for the hydrogenation of FUR to FOL than the copper chromite industrially used [13]. This process was patented by DuPont in 1932 and then was employed by the Quaker Oats Company, attaining a FOL yield of 99% (170 °C) [2]. The furfural hydrogenation reaction is very attractive since, besides FOL, other valuable compounds can be obtained, such as 2-methylfuran (2-MF), tetrahydrofuran (THF), and 2-methyltetrahydrofuran (2-MTHF) (Scheme 1). For this purpose, different materials have been reported as efficient catalysts for the FUR hydrogenation. In particular, transition metal-based catalysts, e.g., Co, Ni, Cu, Pd, and Pt [14–20], have been postulated as potential alternatives to replace the traditional copper chromite.



Scheme 1. Chemical scheme of the possible products obtained from the hydrogenation of furfural (FUR).

A key parameter in determining the selectivity of catalysts towards FOL is the hydrogenating capacity of the transition metal used as active phase. Thus, catalysts based on Group VIII transition metals, such as Pd, Pt, or Ni, due to their high hydrogenating capacity, tend to open the furan ring, or to favor the decarbonylation process. However, Cu-based ones, with a poorer hydrogenating capacity, only attack the carbonyl group of FUR, leading to FOL and 2-MF as main products. In previous studies, Sithisa et al. carried out the hydrogenation of FUR over Cu, Pd, and Ni catalysts supported on SiO₂, at 230 °C and atmospheric pressure, reaching a FUR conversion about 75% for all catalysts [21]. Cu-based catalysts did not cause hydrogenation of the furan ring and thus led mostly to FOL (98%), with a small amount of MF (2%). However, Pd-based catalysts provided mainly furan (60%) with some THF (20%) and FOL (14%), whereas Ni-based catalysts yield products resulting from the hydrogenation and furan ring opening, with a wider range of products. On the other hand, Nagaraja et al. reported the use of Cu/MgO and Cu-MgO-Cr₂O₃ catalysts to attain maximum yield of FOL (>98%) [22,23]. Similar yields of FOL were obtained by several authors using the commercial copper chromite catalyst, under high reaction temperature and hydrogen pressure [14,24]. Unfortunately, the commercial catalyst

presents numerous disadvantages, since it is not environmentally friendly due to the presence of chromium, undergoes a strong deactivation, and works under more drastic catalytic conditions.

The influence of synthesis method of catalysts is also known to be an important factor influencing the catalytic behavior. Thus, Nagaraja et al. studied Cu/MgO catalysts prepared by several synthetic methods: coprecipitation, solid-solid wetting, and impregnation [22]. The highest yield of FOL was obtained for the Cu/MgO catalyst synthesized by coprecipitation, due to its larger amount of available surface Cu⁰ sites, attaining a FUR conversion of 98%, with a FOL selectivity of 98%, without any deactivation after 5 h TOS. These authors concluded that the interaction of Cu particles and the oxygen vacancies of MgO must have a beneficial effect on the catalytic performance. This highlights the importance of the support, so it is necessary to study and optimize parameters, such as the metal-support interaction and morphology of metal particles, because it is well known that partially reducible supports can modify the electronic density of the catalyst surface.

Another challenge in this field is to prevent the catalyst deactivation, due to the sintering of Cu particles, as well as the deposition of carbonaceous species on active sites as a consequence of the strong interaction between FUR and FOL molecules with metal copper sites [2,7]. In this sense, the selection of the support is also a key parameter in determining the catalytic behavior because, in addition to dispersing the metallic particles to increase the number of accessible active centers, the modification of the electronic density of metal can affect the selectivity and catalyst deactivation. It is clearly described that the acid-base behavior of the support influences the dispersion of metal particles. Thus, acidic supports, such as silica, highly disperse the metallic phase, although the acidity must be modulated, since the presence of a large proportion of acid sites can favor polymerization processes. The use of amphoteric or basic supports, such as ZnO and MgO, favors metal-support interaction, which can increase the number of available active centers and so the catalytic activity, as well as the resistance to deactivation due to a weaker interaction with FUR molecules. Thus, different supports have been used for the preparation of Cu-based catalysts: SiO₂ [16,25–27], Al₂O₃ [25,28], MgO [22,23,29,30], ZnO [25,31–33], and CeO₂ [34], and their catalytic activity in FUR hydrogenation has been evaluated. In this sense, our research group has recently showed that the strong interaction of Cu⁰ sites with the amphoteric ZnO avoids the deactivation of the Cu species by a sintering process, especially for the Cu/ZnO catalyst with the lowest metal content, which still shows a FOL yield of 60 mol% after 24 h of TOS [31]. The deactivation by sintering has also been ruled out for the Cu⁰ species dispersed on CeO₂. These Cu/CeO₂ catalysts showed high metal surface area, even for catalysts with high copper content, which reached a FUR conversion of 83%, after 5 h TOS at 190 °C [34]. Moreover, we have also studied the use of clays (bentonite and sepiolite), which are abundant, versatile, and inexpensive natural materials, as supports for copper catalysts [35]. Although these catalysts showed high yields of FOL (72%) after 5 h of TOS at 210 °C, they suffer a progressive deactivation along the TOS. However, a deeper study is required since the use of copper as active phase and clay minerals as support is a competitive and sustainable catalytic system for larger scale application, in such a way that it is environmentally benign due to the absence of chromium in its composition.

Thus, inspired by the above results obtained by our research group in FUR hydrogenation using clay minerals as support [35], the present work deals with the analysis of the influence of the incorporation of several metal oxides, such as MgO, ZnO, and CeO₂, on the catalytic behavior of Cu⁰ catalysts, supported on an inexpensive fibrous phyllosilicate, like sepiolite, in the vapor-phase hydrogenation of FUR to FOL. In all cases, catalytic precursors were obtained by simultaneous coprecipitation of Cu²⁺ species and Mg²⁺, Zn²⁺, or Ce⁴⁺ species in the presence of the sepiolite mineral, a quick and economical method of synthesis in a single step.

2. Catalytic results

2.1. Effect of Oxide-Sepiolite Support

In previous works, it was demonstrated that the interaction between an amphoteric or basic oxide, used as support, and Cu^0 sites enhances the catalytic behavior of Cu-based catalysts in the vapor-phase FUR hydrogenation [22,23,27,31,34]. In this sense, the combined presence of a metal oxide (MgO , ZnO , or CeO_2) and sepiolite as support of metallic Cu species has initially been evaluated. Thus, the catalytic behavior of copper-based catalysts with metal oxide species incorporated in the same step and supported on sepiolite (1CuMgOSep , 1CuZnOSep , and $1\text{CuCeO}_2\text{Sep}$), Cu^0 catalysts dispersed on metal oxides (1CuMgO , 1CuZnO , and 1CuCeO_2), and Cu^0 catalysts supported on sepiolite (CuSep) catalysts were compared. Only FOL and MF were detected as products, as expected for Cu-based catalysts, due to the low hydrogenating capacity that favors the formation of products where the cleavage of C–C bonds is not involved [36–38]. Figure 1 and Table 1 reveals that Cu catalysts with metal oxides species and supported on sepiolite exhibited a much higher FUR conversion than those catalysts synthesized without sepiolite, or a Cu-based catalyst supported on sepiolite. The beneficial effect of both metal oxide species and sepiolite on metal copper sites is ascribed to the modification of their electronic density, which can play an important role in the hydrogenation of FUR in vapor phase, due to the synergy between the metal oxide and sepiolite [22,31,34]. In all cases, a slight deactivation with TOS was observed, although in lower proportion than that observed in previous research using similar supports [35]. In the presence of MgO (Figure 1A), a notable improvement of the catalytic activity was observed, since the FUR conversion increases from about 20% for 1CuMgO to 73% for 1CuMgOSep , containing sepiolite, after 5 h of TOS at 210°C . A similar trend was found for catalysts with ZnO , although higher conversion values are reached. Thus, 1CuZnO attained a FUR conversion of 54%, while 1CuZnOSep showed the highest conversion values, with 80% after 5 h TOS. Finally, the catalysts with CeO_2 (Figure 1A) follow a similar pattern, since the FUR conversion increases from 46% for 1CuCeO_2 to 67% for $1\text{CuCeO}_2\text{Sep}$.

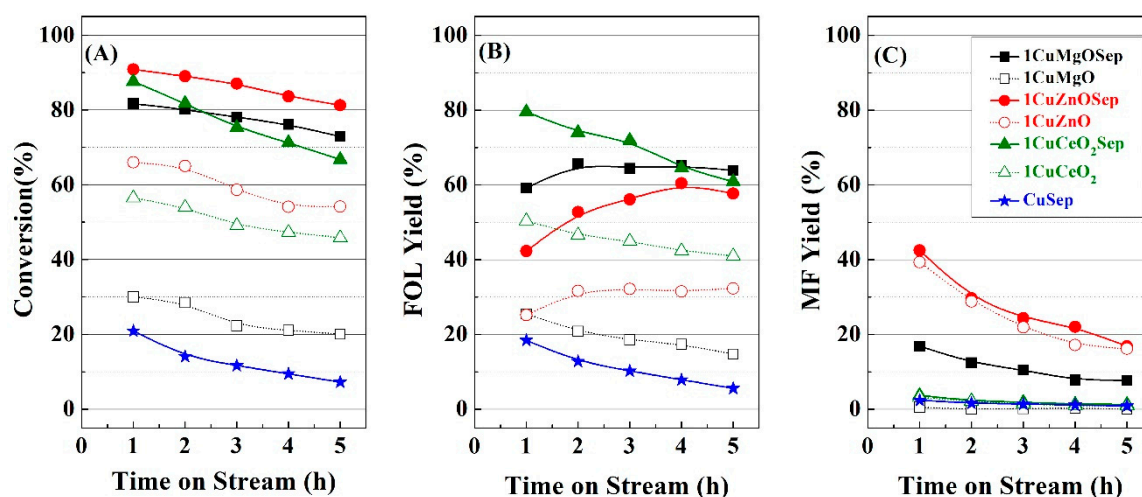


Figure 1. Furfural (FUR) conversion (A), furfuryl alcohol (FOL) yield (B) and 2-methylfuran (MF) yield (C) of Cu supported on metal oxides with (closed symbols) and without sepiolite (open symbols), with Cu/M molar ratio of 1. (Catalytic conditions: Mass of catalyst = 0.15 g, Reaction temperature = 210°C , Pressure = 0.1 MPa, H_2 -flow = 10 mL min^{-1} , Fed flow = $2.3\text{ mmol FUR h}^{-1}$).

As was indicated previously, both FOL and MF were the products detected, since the Cu sites only attack the carbonyl group of the FUR molecule [21,36]. Nonetheless, the analysis of the carbon balance indicated the presence of less than 10% of non-detected products, probably due to the strong adsorption of FUR or FOL on the surface of the catalysts, as was reported in previous research [36–38]. In all cases, FOL was obtained in a higher proportion, mainly in the case of catalysts containing MgO

and CeO₂. Contrarily, catalysts with ZnO favored the formation of MF, mainly in the first hours of TOS. Nonetheless, the decrease in the MF yield was accompanied by a rise in FOL production. This fact could indicate that active sites involved in the hydrogenolysis process, which converts FOL into MF, are more susceptible to deactivation due to the formation of H₂O as a byproduct, which could favor the oxidation of metal copper species. However, the hydrogenation reaction (FUR → FOL) is less sensitive to deactivation. This fact has been associated to the formation of water in the hydrogenolysis process, that can oxidize the active phase, and favor the metal sintering or the formation of carbonaceous deposits responsible of catalyst deactivation. From this study, it can be concluded that the higher FOL yields (57–63%) after 5 h of TOS at 210 °C were obtained for copper catalysts with oxide species and supported on sepiolite.

Table 1. FUR conversion, FOL yield, and MF yield in the FUR hydrogenation of Cu supported on metal oxides with and without sepiolite, with Cu/M molar ratio of 1. (Catalytic conditions: Mass of catalyst = 0.15 g, Reaction temperature = 210 °C, Pressure = 0.1 MPa, Time on stream = 5 h, H₂-flow = 10 mL min^{−1}, Fed flow = 2.3 mmol FUR h^{−1}).

| Catalyst | Conv (%) | Y _{FOL} (%) | Y _{MF} (%) |
|-------------------------|----------|----------------------|---------------------|
| 1CuMgO | 20 | 15 | <1 |
| 1CuZnO | 54 | 32 | 16 |
| 1CuCeO ₂ | 45 | 41 | 1 |
| 1CuMgOSep | 73 | 64 | 8 |
| 1CuZnOSep | 81 | 58 | 17 |
| 1CuCeO ₂ Sep | 66 | 61 | 1 |

2.2. Influence of the Reaction Temperature

Once proven that the use of oxide species dispersed on sepiolite allowed obtaining supported copper catalysts leading to the highest FUR conversion, these catalysts were selected to carry out a detailed analysis. Considering that the FUR boiling point is 161.7 °C, the lowest reaction temperature selected was 170 °C. The catalytic activity increases directly with the reaction temperature, reaching the highest FUR conversion between 190–210 °C (Figure 2 and Table 2). A higher reaction temperature (230 °C) decreased the catalytic activity, mainly in the case of 1CuZnOSep and 1CuCeO₂Sep, where FUR conversion values of 68% and 42% were obtained, respectively, after 5 h of TOS. However, 1CuMgOSep was more resistant to the increase in temperature, achieving a conversion of 80% under similar experimental conditions (Figure 1A). These catalytic behaviors are in agreement with those shown in the literature, since several authors have predicted a volcano profile when the reaction temperature is increased, due to desorption of FUR molecules from active sites at higher reaction temperature before the hydrogenation process [35,39].

In all cases, FOL was the main product, although the MF yield enhanced with the reaction temperature (after the first hours of TOS), especially for 1CuMgOSep and 1CuZnOSep catalysts. The MF yield obtained with the 1CuCeO₂Sep catalyst can be considered as negligible, in agreement with data previously reported for Cu⁰ species dispersed on CeO₂ with different Cu/Ce molar ratios [34]. This fact could confirm that the hydrogenolysis reaction is favored at higher temperatures. The analysis of the catalytic behavior after 5 h of TOS (Table 2) revealed a decrease in FUR conversion, mainly for the 1CuCeO₂Sep catalyst. Regarding the selectivity pattern, the main product was FOL, with MF being a minor product. The catalytic data (Figure 2) pointed out that a decrease in MF yield is accompanied by the increase in FOL yield due to the deactivation of active sites responsible of the hydrogenolysis process. This fact is more pronounced for 1CuMgOSep and 1CuZnOSep catalysts at higher reaction temperature. The decrease in the MF yield along the TOS could be ascribed to a possible sintering of copper species, which is favored at higher temperature, due to the oxidation of Cu species by the H₂O formed in the hydrogenolysis reaction and the FUR polymerization.

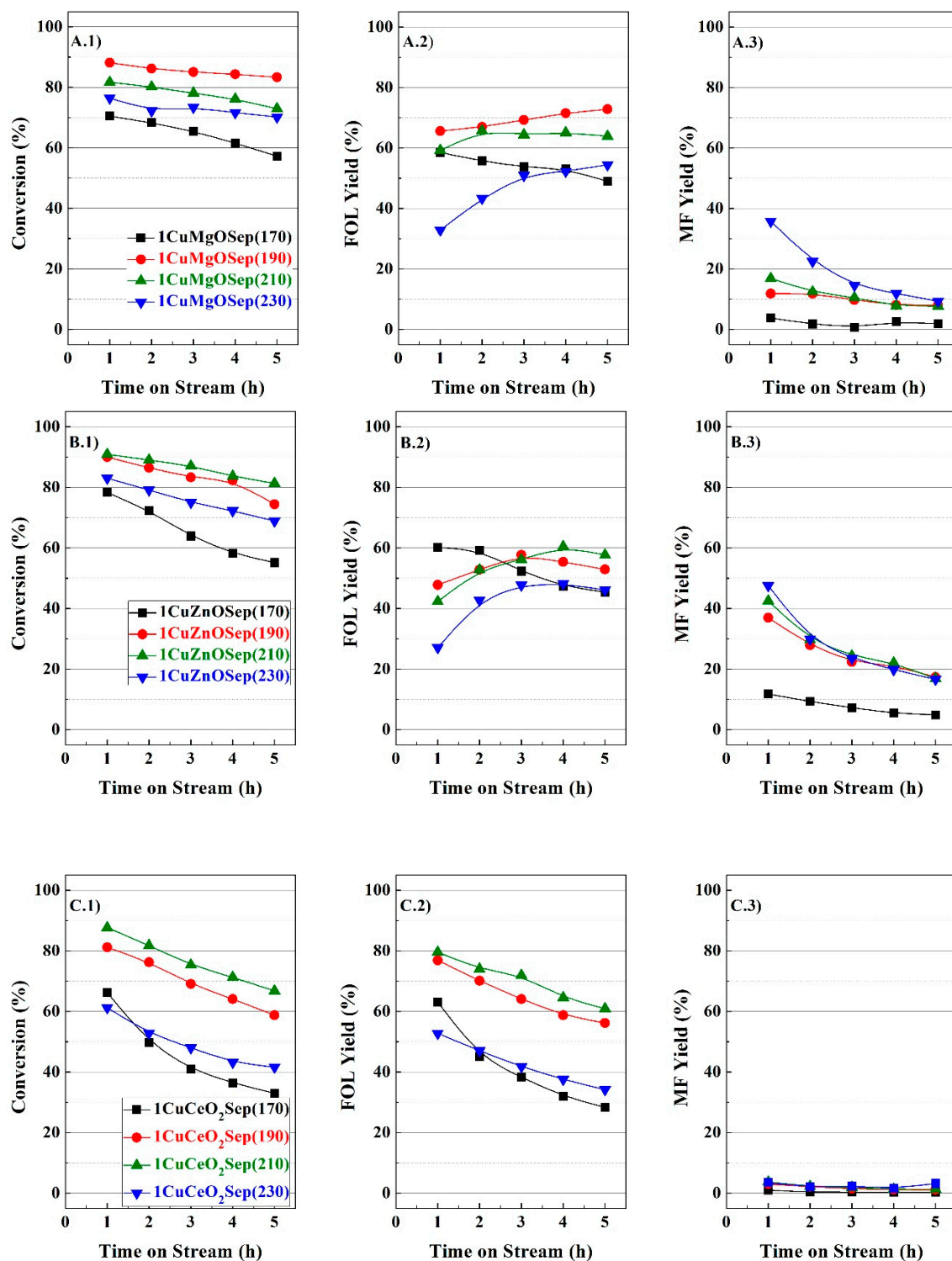


Figure 2. FUR conversion (1), FOL yield (2), and MF yield (3) of Cu supported on MgO (A), ZnO (B) and CeO₂ (C) metal oxides with sepiolite (Cu/M molar ratio of 1). Comparative catalytic study in the FUR hydrogenation for Cu supported on MgO, ZnO, and CeO₂ with a Cu/M molar ratio of 1 and supported on sepiolite. (Catalytic conditions: Mass of catalyst_t = 150 mg, Reaction temperature = 170–230 °C, H₂-flow = 10 mL min^{−1}, Fed flow = 2.3 mmol FUR h^{−1}).

Table 2. FUR conversion, FOL yield, and MF yield in the FUR hydrogenation of Cu supported on metal oxides with sepiolite, with Cu/M molar ratio of 1. (Catalytic conditions: Mass of catalyst = 0.15 g, Reaction temperature = 170–230 °C, Pressure = 0.1 MPa, Time on stream = 5 h, H₂-flow = 10 mL min^{−1}, Fed flow = 2.3 mmol FUR h^{−1}).

| Catalyst | Conv (%) | Y _{FOL} (%) | Y _{MF} (%) |
|------------------------------|----------|----------------------|---------------------|
| 1CuMgOSep(170) | 57 | 49 | 2 |
| 1CuMgOSep(190) | 83 | 73 | 8 |
| 1CuMgOSep(210) | 73 | 64 | 8 |
| 1CuMgOSep(230) | 70 | 52 | 10 |
| 1CuZnOSep(170) | 55 | 45 | 5 |
| 1CuZnOSep(190) | 74 | 53 | 17 |
| 1CuZnOSep(210) | 81 | 58 | 17 |
| 1CuZnOSep(230) | 69 | 46 | 17 |
| 1CuCeO ₂ Sep(170) | 33 | 28 | <1 |
| 1CuCeO ₂ Sep(190) | 59 | 56 | <1 |
| 1CuCeO ₂ Sep(210) | 68 | 61 | 1 |
| 1CuCeO ₂ Sep(230) | 42 | 51 | 5 |

2.3. Study of the Cu/M Molar Ratio for the CuMOxSep Catalysts

Next, the influence of the Cu/M molar ratio ($x = 0.4, 1$ and 2.5) of the Cu-based catalysts was evaluated. Figure 3 and Table 3 point out that all catalysts showed both a high FUR conversion and a higher yield of FOL than MF. For x CuMgOSep catalysts (Figure 3A), in spite of using different Cu/Mg molar ratios, the catalysts present very similar conversion values (81–86%) after 1 h of TOS at 210 °C. However, these catalysts underwent a slight deactivation along the TOS. In all cases, x CuMgOSep catalysts provide mainly FOL, especially when the Cu/Mg molar ratio decreases and over longer reaction times, due to the deactivation of active sites, where the hydrogenolysis reaction occurs.

Table 3. FUR conversion, FOL yield, and MF yield in the FUR hydrogenation of Cu supported on metal oxides with sepiolite, with Cu/M molar ratio of 0.4–2.5. (Catalytic conditions: Mass of catalyst = 0.15 g, Reaction temperature = 210 °C, Pressure = 0.1 MPa, Time on stream = 5 h, H₂-flow = 10 mL min^{−1}, Fed flow = 2.3 mmol FUR h^{−1}).

| Catalyst | Conv (%) | Y _{FOL} (%) | Y _{MF} (%) |
|---------------------------|----------|----------------------|---------------------|
| 0.4CuMgOSep | 73 | 66 | 2 |
| 1CuMgOSep | 73 | 64 | 8 |
| 2.5CuMgOSep | 68 | 51 | 12 |
| 0.4CuZnOSep | 62 | 58 | 4 |
| 1CuZnOSep | 81 | 58 | 14 |
| 2.5CuZnOSep | 68 | 55 | 5 |
| 0.4CuCeO ₂ Sep | 37 | 28 | 7 |
| 1CuCeO ₂ Sep | 68 | 61 | 1 |
| 2.5CuCeO ₂ Sep | 73 | 69 | 1 |

With regard to the x CuZnOSep catalysts (Figure 3B), the highest conversion value was obtained for 1CuZnOSep, which suffers a less pronounced deactivation along the TOS in comparison to other catalysts. This catalyst was the most selective to MF, attaining a yield of 41% at shorter TOS; however, MF yield decreases, and the production of FOL concomitantly increases, with TOS as a

consequence of the gradual deactivation of the sites involved in the second step of the sequential process: $\text{FUR} \rightarrow \text{FOL} \rightarrow \text{MF}$.

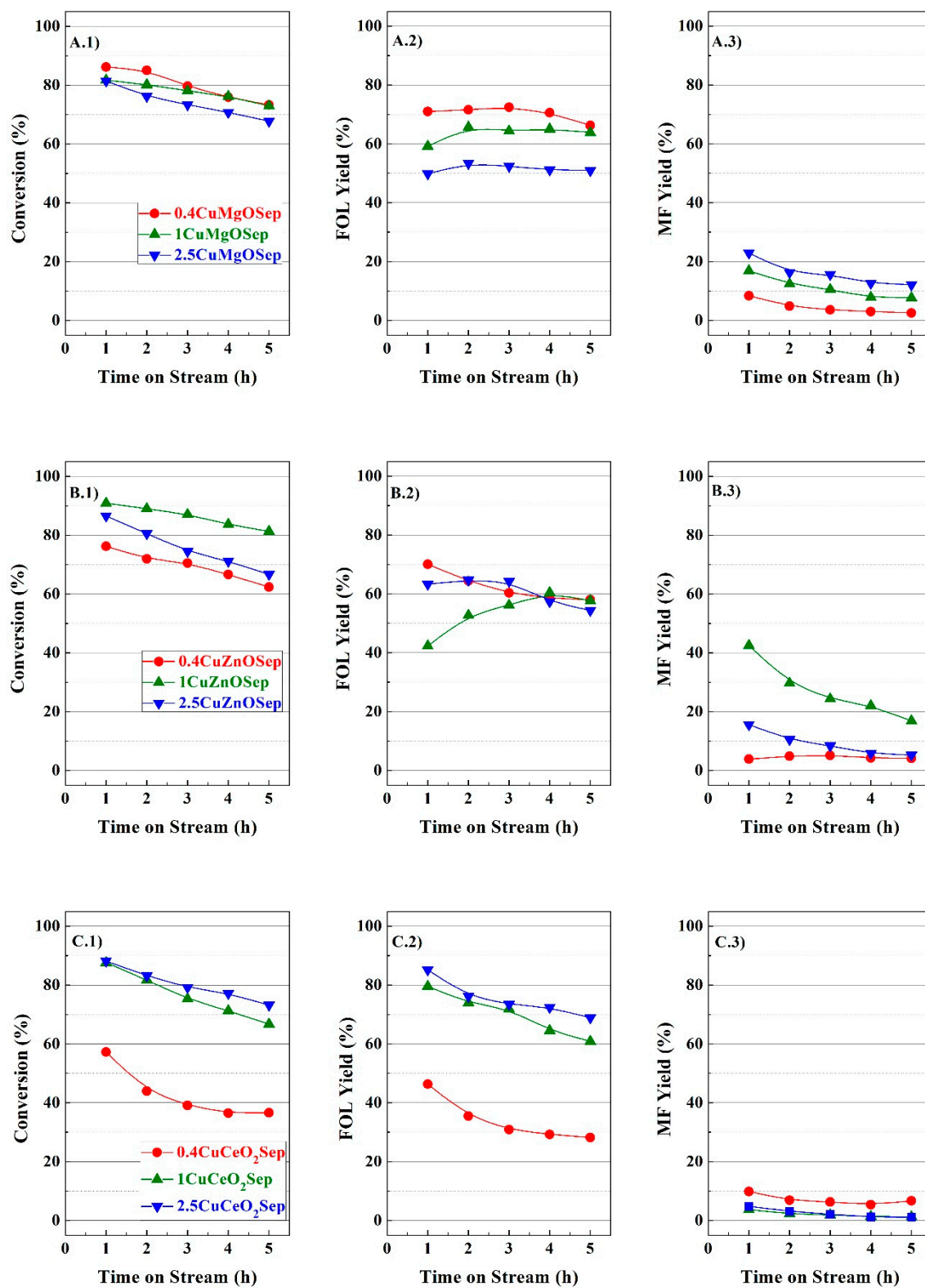


Figure 3. FUR conversion (1), FOL yield (2), and MF yield (3) of Cu supported on MgO (A), ZnO (B), and CeO₂ (C) metal oxides with sepiolite (Cu/M molar ratio of 0.4–2.5). (Catalytic conditions: Mass of catalyst_t = 150 mg, Reaction temperature = 210 °C, Pressure = 0.1 MPa, H₂-flow = 10 mL min^{−1}, Fed flow = 2.3 mmol FUR h^{−1}).

For the $x\text{CuCeO}_2\text{Sep}$ catalysts (Figure 3C), it is noteworthy that the sample with lowest Cu/Ce molar ratio, i.e., the $0.4\text{CuCeO}_2\text{Sep}$ sample, showed the poorest conversion and a greater susceptibility to deactivation, which is in agreement with data reported in the literature [34]. The activity of the $x\text{CuCeO}_2\text{Sep}$ catalysts directly increases with the Cu/Ce molar ratio, attaining a very similar catalytic behavior for $1\text{CuCeO}_2\text{Sep}$ and $2.5\text{CuCeO}_2\text{Sep}$, which are highly selective to FOL.

2.4. Study of the Stability

In an additional study, one of the most promising catalyst ($1\text{CuMgO}\text{Sep}$) was selected to be evaluated for longer TOS (Figure 4). It can be observed how the FUR conversion decreases gradually with TOS, reaching a conversion of 55% after 24 h of TOS. With regard to the yield, FOL formation slightly increases during the first two hours as a result of the decline of the MF yield. Then, FOL yield follows the same trend as that observed for the FUR conversion, attaining a yield of 51% after 24 h of TOS.

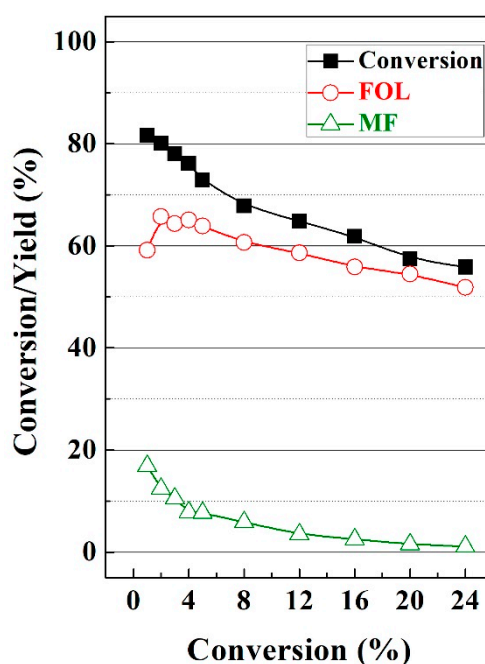


Figure 4. FUR conversion, FOL yield, and MF yield of $1\text{CuMgO}\text{Sep}$ catalysts (Cu/Mg molar ratio = 1) after 24 h of TOS. (Catalytic conditions: Mass of catalyst = 0.15 g, Reaction temperature = $210\text{ }^{\circ}\text{C}$, Pressure = 0.1 MPa, H_2 -flow = 10 mL min^{-1} , Fed flow = $2.3\text{ mmol FUR h}^{-1}$).

3. Characterization of Catalysts

From the catalytic study, it is feasible to infer a positive effect of the incorporation of metal oxides to copper supported on sepiolite catalysts in the vapor-phase hydrogenation of FUR, and the Cu/M molar ratios have been optimized for each family of catalysts. Therefore, it is necessary to characterize these catalysts to explain this beneficial effect.

Firstly, the reduction profiles of precursors have been determined by H_2 -TPR (Figure 5). It is well known that the reducibility of CuO species directly depends on the synthesis method, the interaction with the support and the reducibility of the support [37,39]. Several authors have indicated that the reduction of copper takes place in a sequential process ($\text{Cu}^{2+} \rightarrow \text{Cu}^+ \rightarrow \text{Cu}^0$). However, in most cases, it is difficult to differentiate between these two different reduction peaks due to morphological/structural differences in CuO entities involved in the reduction process [40].

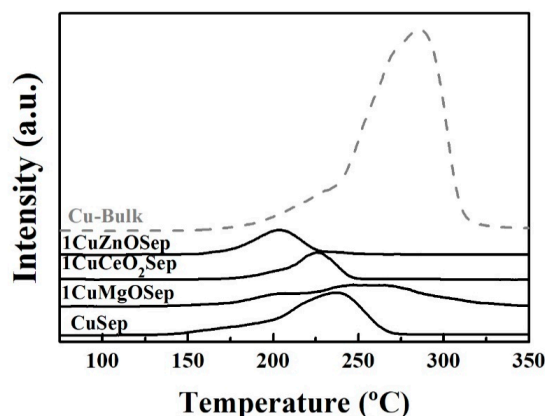


Figure 5. H₂-TPR of the Cu-based catalysts with oxide species incorporated (MgO, CeO₂, ZnO) and supported on sepiolite.

For the bulk CuO, two different reduction peaks can be observed: the reduction of smaller CuO particles starts at about 164 °C, whereas the maximum H₂ consumption at 285 °C is assigned to bigger CuO particles. This value is higher than those observed for catalysts supported on sepiolite, pointing out the formation of smaller dispersed Cu nanoparticles, which are easily reduced [35]. Thus, the maximum reduction temperature is slightly displaced at lower temperature (237 °C) for the CuSep material.

In the case of catalysts containing ZnO, i.e., 1CuZnO and 1CuZnOSep, both display a similar profile. Thus, the 1CuZnO material showed a H₂ consumption signal centered about 200 °C, as previously reported [31], similar to the profile corresponding to 1CuZnOSep, as can be observed in Figure 5. This peak is only associated with the reduction of CuO species since the reduction of ZnO occurs at much higher temperature. The presence of ZnO and sepiolite in the catalyst might facilitate the reduction of the Cu²⁺ species due to the formation of dispersed CuO nanostructures, which should be reduced more easily.

With regard to the MgO-based catalysts, previous studies carried out for CuO supported on MgO, obtained by a coprecipitation method, have revealed that H₂ consumption for reduction of copper species took place in a wide range of temperatures (200–400 °C), as was observed for the 1CuMgOSep catalyst (Figure 5). This fact suggests the presence of both highly dispersed small CuO particles with different interaction with the support (200–230 °C) and larger particles (275 °C).

In the case of the catalysts based on CeO₂, the reducibility of Ce(IV) must be considered, as has been previously reported [34]. The formation of a CuO/CeO₂ system in the 1CuCeO₂ material ameliorates the reducibility of CuO species as a consequence of the oxygen mobility promoted by the ceria, which favors the spillover process in interfacial surfaces. The H₂-TPR profile reveals that there is a first H₂ consumption signal centered about 150 °C attributed to the reduction of highly dispersed CuO species in contact with CeO₂, and a more intense second signal about 200 °C associated to the reduction of bulk CuO species. The profile corresponding to the catalyst containing sepiolite (1CuCeO₂Sep) is very similar to that of 1CuCeO₂, but the signals are displaced at higher temperatures, about 200 °C for the first H₂ consumption and 225 °C for the second one.

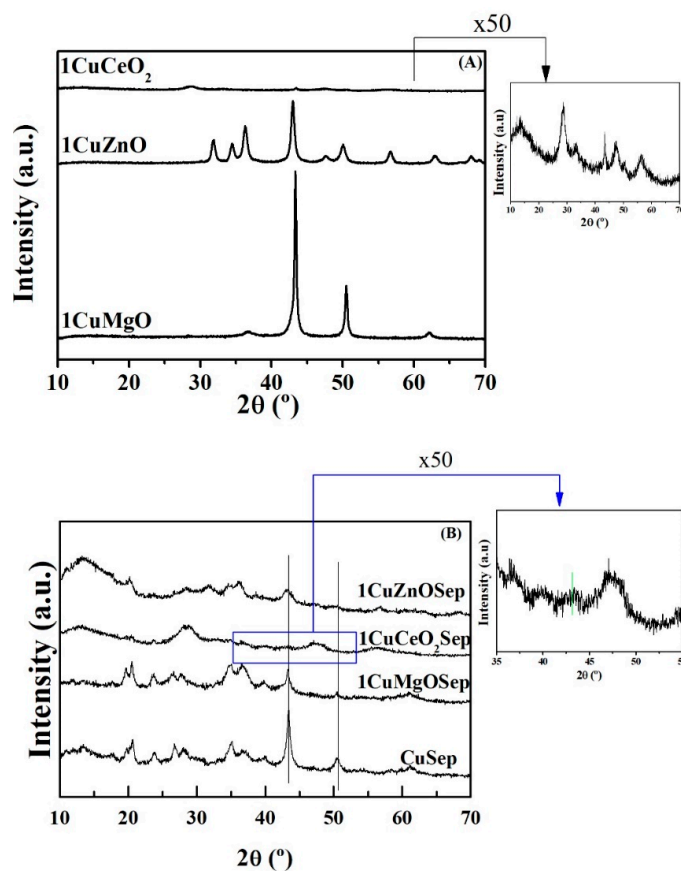
The analysis of the H₂-TPR profiles revealed a H₂ consumption of 2364 μmol g^{−1} for 15CuSep, while 1CuMgOSep, 1CuZnOSep, and 1CuCeO₂Sep consumed 1775 μmol g^{−1}, 1624 μmol g^{−1}, and 1378 μmol g^{−1}. These data suggest that the incorporation of MO_x species causes a decrease in the amount of Cu⁰ sites available for the reaction. This fact is more pronounced as the atomic weight of the M species (M = Mg, Zn, Ce) increases. However, the values are relatively close to the theoretical ones, so the total reduction of Cu species can be confirmed (Table 4).

Table 4. H₂-consumption of the Cu-based catalysts supported on mixed oxides and sepiolite (Cu/M molar ratio of 1).

| Catalyst | H ₂ -Consumption ($\mu\text{mol g}^{-1}$) | |
|-------------------------|--|------------------|
| | Experimental Data | Theoretical Data |
| CuSep | 2364 | 2363 |
| 1CuMgOSep | 1775 | 1889 |
| 1CuZnOSep | 1624 | 1763 |
| 1CuCeO ₂ Sep | 1378 | 1496 |

According to this reducibility study, the temperature selected to reduce the catalytic precursors of this series of catalysts was 300 °C. This temperature was maintained during 1 h to favor the total reduction of precursors.

X-ray diffraction patterns of the Cu-based catalysts after its reduction at 300 °C are shown in Figure 6. The diffraction peaks located about $2\theta = 43.6$ and 50.6° can be attributed to Cu⁰ (PDF 00-004-0836), while the absence of diffraction peaks associated to CuO ($2\theta = 32.5, 35.5, 38.7, 48.8, 53.5, 58.3, 61.6, 66.2$, and 68.1° , PDF 00-048-1548) corroborates the complete reduction of precursors under the selected reduction conditions. Considering that sepiolite is a natural clay mineral, XRD shows a set of bands located at $2\theta = 20$ and 40° , indicating that sepiolite displays high crystallinity [41,42]. In addition, the diffraction peak located at 60.8° (1.52 \AA) confirms the presence of a trioctahedral phyllosilicate, which implies high proportion of MgO species in the octahedral sheet of the sepiolite.

**Figure 6.** X-ray diffraction (XRD) patterns of the Cu-based catalysts supported on mixed oxides (A) and supported on mixed oxides and sepiolite (B) (Cu/M molar ratio of 1).

Moreover, the 1CuZnO catalyst exhibits peaks at $2\theta = 31.8, 34.4, 36.2, 47.6, 56.7$, and 63.0° , which correspond to the hexagonal ZnO phase (PDF 00-036-1451) together with signals assigned to Cu^0 crystallites. These diffraction peaks are also present in the corresponding catalyst with sepiolite, 1CuZnOsep, but their intensity is much lower, which indicates a higher dispersion of metal copper and ZnO particles when the sepiolite is employed as support. For the 1CuCeO₂ and 1CuCeO₂sep catalysts, peaks at $2\theta = 28.5, 33.4, 47.5, 56.5, 59.2$, and 61.6° are assigned to the cubic fluorite-type structure of the CeO₂ crystallites (PDF 00-034-0394), whereas those of metal Cu^0 are barely distinguished. In the enlarged figure, it can be observed that these signals are almost not observed for the catalyst containing sepiolite, which is reflected in the smallest metal particle size (3.3 nm) for this catalyst (Table 5). The intensity of Cu^0 peaks is very high for the 1CuMgO catalyst, whilst these are much less intense for the material containing sepiolite (1CuMgOsep). In general, Cu^0 diffraction peaks are less intense for the catalysts containing both metal oxide and sepiolite. This would point out their lower crystallinity, due to smaller particle sizes, as corroborated by using the Williamson–Hall method (Table 5) [43]. These smaller particle sizes of the Cu-based catalysts with oxide species and dispersed on sepiolite, compared to those supported on metal oxides, can explain the beneficial effect for copper catalysts in the furfural hydrogenation, because the most suitable dispersion of metal Cu^0 sites is achieved. The 1CuCeO₂sep catalyst has a much smaller copper particle size (3.3 nm) than CuZnOsep (10.1 nm) and 1CuMgOsep (13.0 nm) catalysts. The N₂O titration (Table 5) shows how all catalysts display similar metallic surface (92.1–98.8), so the catalytic data could be compared.

Table 5. Textural properties, Cu^0 particle size, dispersion of Cu^0 particles, and metallic surface of the Cu-based catalysts supported on mixed oxides and sepiolite (Cu/M molar ratio of 1).

| Catalysts | S_{BET} ($\text{m}^2 \cdot \text{g}^{-1}$) | V_p ($\text{cm}^3 \cdot \text{g}^{-1}$) | d_{Cu^0} (nm) ^a | D (%) ^b | S_{Cu^0} ($\text{m}^2_{\text{Cu}} \cdot \text{g}^{-1}_{\text{Cu}}$) ^b | d_{Cu^0} (nm) ^b | Acid Sites ($\mu\text{mol g}^{-1}$) ^c |
|-------------------------|--|--|--|-----------------------|--|--|---|
| 1CuCeO ₂ sep | 113 | 0.223 | 3.3 | 10 | 92.1 | 7.3 | 44 |
| 1CuZnOsep | 98 | 0.220 | 10.1 | 10 | 93.1 | 7.2 | 89 |
| 1CuMgOsep | 71 | 0.147 | 13.0 | 7 | 98.0 | 6.9 | 62 |

^a Crystal size from Williamson–Hall equation ($2\theta = 43.5^\circ$). (Crystal size of 1CuCeO₂: 13.4 nm, 1CuZnO: 17.2 nm and 1CuMgO: 36.1 nm); ^b Titration with N₂O; ^c Estimated from NH₃-TPD.

The morphology of the catalysts was determined by TEM (Figure 7). The TEM micrographs show how the sepiolite displays a fibrous structure. On its surface, the presence of deposited Cu particles is noteworthy (Figure 7A). These Cu particles display a spherical morphology with a variable diameter between 5 and 25 nm. The incorporation of MgO, ZnO, or CeO₂ species also leads to the deposition of these species together with the Cu^0 particles (Figure 7B–D). In all cases, both the particles of Cu^0 and the particles of MO_x are in intimate contact with each other, as indicated in Figure 8.

Cu^0 and MO_x particles present a variable size (Figure 8), although the bigger Cu particles observed in the Cu-based catalyst supported on sepiolite, have not been detected in these catalysts with MO_x species. On the other hand, the incorporation of the MO_x species favors an increase of the dispersion of the Cu species. This fact also implies a decrease of the Cu content (in wt.%), which is related to a decrease of the crystallinity in the catalytic system, as was previously detected in the XRD data (Figure 6). It is noteworthy that the 1CuMgOsep catalyst displays Cu particles more agglomerated than those observed for 1CuZnOsep and 1CuCeO₂sep catalysts. However, their presence could not be inferred from XRD and N₂O titration. This fact would suggest the existence of Cu particles with variable sizes, which is in agreement with the broad reduction curves obtained in the H₂-TPR study.

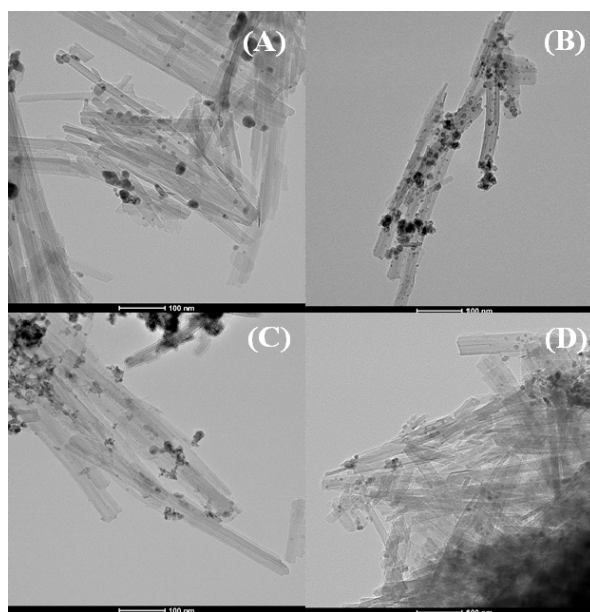


Figure 7. Transmission electron microscopy (TEM) micrographs of CuSep (A), 1CuMgOSep (B), 1CuZnOSep (C), and 1CuCeO₂Sep (D) (Magnification: 100 nm).

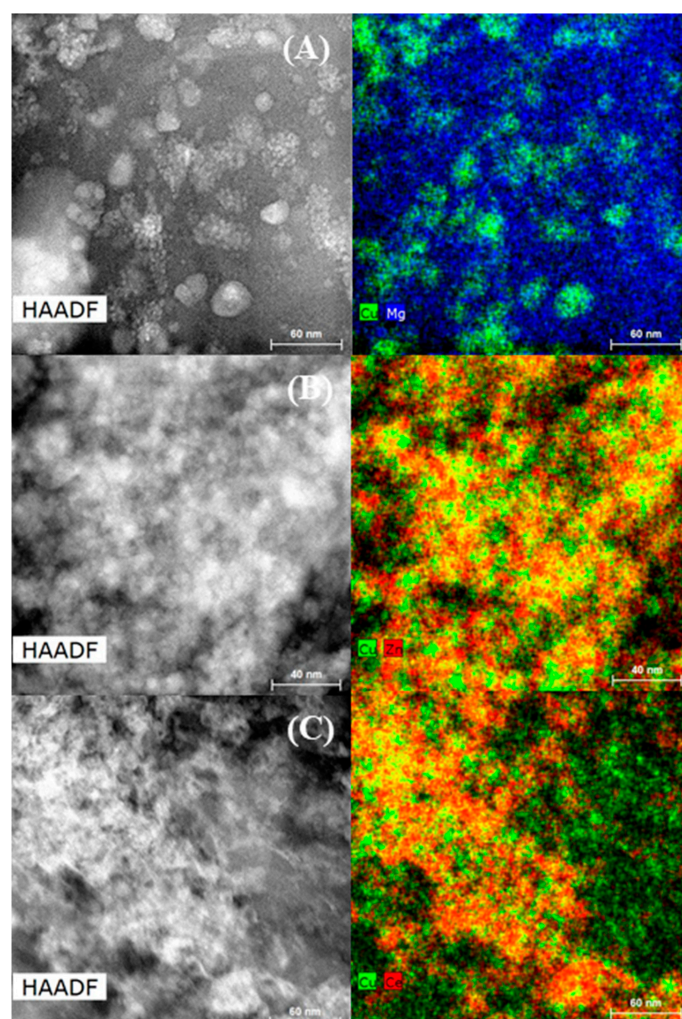


Figure 8. STEM and Energy Dispersive X-Ray (EDX) Analysis for 1CuMgOSep (A), 1CuZnOSep (B), and 1CuCeO₂Sep (C).

The textural parameters of the Cu-based catalysts were determined from their N₂ isotherms (Figure 9A). The catalysts display Type II isotherms, which are ascribed to macroporous solids, which indicates the N₂ adsorbed at high relative pressure [44]. All the catalysts display similar profiles, except in the case of the 1CuCeO₂Sep catalyst, which shows a strong increase in N₂ adsorption at higher relative pressure.

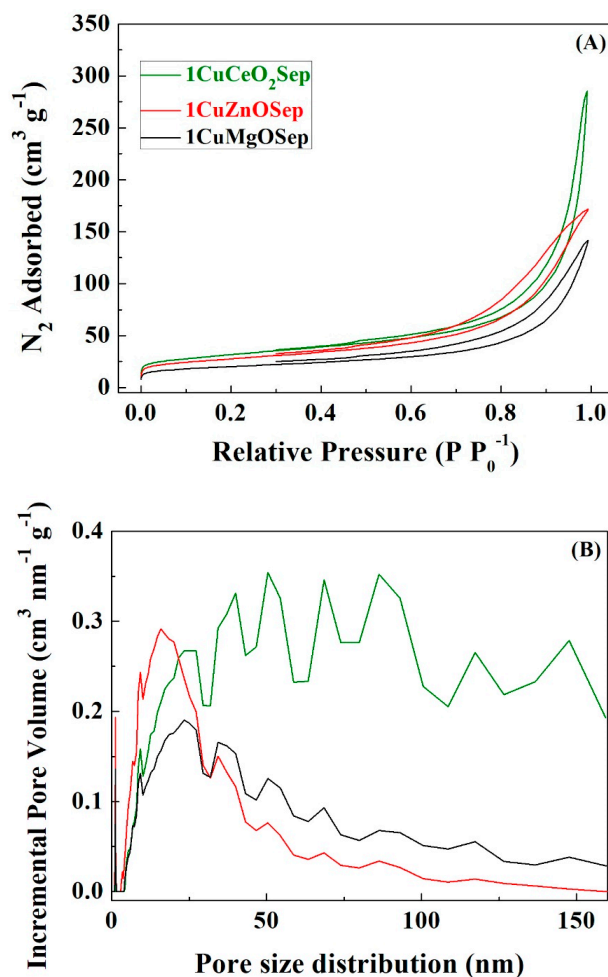


Figure 9. N₂ adsorption-desorption isotherms at −196 °C (A) and pore size distributions estimated by the Density Functional Theory (DFT) method (B) of the Cu-based catalysts with oxide species and supported on sepiolite (Cu/M molar ratio of 1).

Table 5 summarizes the textural properties of catalysts with metal oxide species and supported on sepiolite, estimated from their N₂ adsorption-desorption isotherms. The formation of smaller particles, as inferred from XRD data, could imply an increase in interparticle voids, in such a way that macropores are generated between adjacent particles. This fact leads to the increase in the specific surface area (S_{BET}) as well as its pore volume (V_{p}). Thereby, the 1CuCeO₂Sep catalyst, which displays the smallest copper particle size (3.3 nm), shows the highest S_{BET} value (113 m² g⁻¹) and pore volume (0.223 cm³ g⁻¹). Therefore, textural characteristics seem to depend on the copper particle size in catalysts.

The pore size distribution profiles, as determined from DFT calculation (Figure 9B) [45], show the existence of microporosity associated with the clay mineral structure. The periodic inversion of tetrahedral positions in sepiolite generates cavities with dimensions of 0.37 nm × 1.06 nm has been reported [46]. These dimensions are appropriate to favor the diffusion of FUR molecules through the channels; however, metal Cu⁰ particles are bigger than these cavities, so it is expected that the FUR hydrogenation takes place on the surface of the sepiolite. On the other hand, the presence of high

macroporosity for 1CuCeO₂Sep is also noteworthy, which may be ascribed to voids between adjacent fibers, metal oxide species, and Cu⁰ particles, being higher when the particle size is smaller, as was previously indicated.

FUR hydrogenation takes place following the sequence: FUR → FOL → MF. The first reaction (FUR → FOL) requires hydrogenating sites, while the second one (FOL → MF) is a hydrogenolysis process, which requires acid sites. Considering this premise, the quantification of acid sites is an important parameter to explain the selectivity pattern. The NH₃-TPD analysis of the natural sepiolite does not show any acidity. It is well known that the substitution of Si⁴⁺ by Al³⁺ in tetrahedral positions of silicates creates acid sites in the resulting aluminosilicate; however, the sepiolite hardly presents Al³⁺ species, since it is a trioctahedral clay mineral, i.e., it possesses a high proportion of Mg²⁺ [41]. This fact implies that the support must exhibit a negligible acidity. The incorporation of metal copper species does not provide any acidity to the catalytic system. When MgO or CeO₂ were incorporated, similar acidity values were obtained, with 62 μmol g^{−1} for 1CuMgOSep and 44 μmol g^{−1} for 1CuCeO₂Sep catalyst (Table 5). In the case of the 1CuZnOSep, the acidity is slightly higher 89 μmol g^{−1}. The obtained data seem to be in agreement with the catalytic activity, since the catalyst with the highest acidity (1CuZnOSep) is also the most selective towards MF. In this way, previous researches have established that the use of low-acidity supports, such as SiO₂, together with small Cu particles favors the hydrogenolysis reaction to MF [25,40,47]. In this sense, Scotti et al. pointed out that the presence of very small Cu⁰ particles, as takes place in the present work, gives rise to catalytically relevant Lewis acidity [47]. However, the support acidity must be modulated, since supports with a high acidity can cause the polymerization of FUR in the vapor phase.

The titration of reduced catalysts with N₂O allows the determination of Cu⁰-dispersion (%D), the metallic surface (S_{Cu⁰}), as well as the diameter of Cu⁰ particles (d_{Cu⁰}) (Table 5). 1CuZnOSep and 1CuCeO₂Sep catalysts display a copper dispersion of 10%, while 1CuMgOSep presents a lower dispersion (7%). With regard to the metallic surface area, 1CuCeO₂Sep exhibits the lowest value, probably due to having the highest molecular weight of the cerium in comparison to magnesium or zinc. Finally, the estimation of the diameter for the Cu⁰ crystals reveals that all catalysts display similar values, between 7.2–9.8 nm. These are not exactly the same as those obtained from XRD data, although they are within the same order of magnitude.

To determinate the chemical composition of the catalyst surface, XPS analysis was carried out (Table 6). In all cases, it is observed the typical binding energies of elements present in trioctahedral phyllosilicates in the Si 2p, Al 2p, Mg 2p, and O 1s core level spectra [48]. In the Cu 2p region, a contribution of about 932.4–932.1 eV is noteworthy, which is attributed to reduced Cu species. The presence of Cu²⁺ species must be discarded since in no case is a broad band observed, about 934.0–935.0 eV, which is ascribed to the shake-up satellite, typical of bivalent species. To distinguish between Cu⁰ and Cu⁺, a Cu_{LMM} Auger line was also evaluated. In all cases, mostly Cu⁰ species (918.0 eV) are detected, confirming the total reduction of Cu(II) species, as shown in the XRD data (Figure 5). From the atomic concentrations reported in Table 2, it can be inferred that the 1CuZnOSep catalyst presents the highest concentration of surface Cu species. These data are in agreement with those obtained from the N₂O titration, where this catalyst showed the highest metallic surface (Table 5). The Cu-based catalysts with oxide species and supported on sepiolite were recovered after the reaction to elucidate the cause of deactivation. The analysis of the Cu 2p core level spectra (Figure 10A) does not reveal any changes in the oxidation state of copper species, since Cu⁰ species remain after the catalytic test (Figure 10B), so the active phase is hardly modified along the TOS. Considering the atomic concentration of the used catalysts (Table 6), the high carbon content on the catalyst surface is striking, mainly for 1CuZnOSep. This fact can be attributed to two possible factors. On one hand, the 1CuZnOSep catalyst presents the highest Cu surface area, so this catalyst also displays the highest proportion of available Cu sites to interact with FUR molecules and generate carbonaceous products. In this sense, some researchers have established that FOL and FUR molecules interact strongly with metal copper sites [36]. On the other hand, 1CuZnOSep displays the highest amount of acid sites,

which are necessary for the hydrogenolysis reaction [25]. This reaction causes the cleavage of the C–O bond, and it can also generate a higher proportion of carbonaceous deposits. Focusing on the Cu content after the reaction, it is noteworthy that the amount of surface copper species follows the trend $1\text{CuZnOSeP} > 1\text{CuMgOSeP} > 1\text{CuCeO}_2\text{SeP}$. These data follow the same trend to that shown in Figure 1 from 3 h of TOS. From these data, it can be inferred that the catalytic activity is related to the electronic density after the first hours of TOS; however, the amount of available Cu species plays a more important role for longer reaction times.

Table 6. Surface atomic concentrations for the Cu-based catalysts with oxide species and supported on sepiolite, before and after vapor-phase FUR hydrogenation (Cu/M molar ratio of 1).

| Catalyst | Atomic Concentrations | | | | | | | | |
|---------------------------|-----------------------|-------|-------|-------|-------|-------|-------|-------|-------|
| | C 1s | O 1s | Mg 2p | Al 2p | Si 2p | Na 1s | Cu 2p | Zn 2p | Ce 3d |
| Fresh catalysts | | | | | | | | | |
| 1CuMgOSeP | 7.32 | 53.93 | 10.44 | 7.97 | 18.37 | 1.87 | 2.27 | - | - |
| 1CuZnOSeP | 6.88 | 51.93 | 8.43 | 7.84 | 15.57 | 2.05 | 2.29 | 3.89 | - |
| 1CuCeO ₂ SeP | 6.55 | 55.97 | 8.64 | 6.52 | 16.69 | 2.64 | 1.87 | - | 2.36 |
| Used catalysts | | | | | | | | | |
| 1CuMgOSeP-u | 34.64 | 38.18 | 7.69 | 5.49 | 10.84 | 1.55 | 1.58 | - | - |
| 1CuZnOSeP-u | 53.26 | 27.76 | 3.11 | 5.32 | 4.51 | 1.49 | 1.99 | 2.00 | - |
| 1CuCeO ₂ SeP-u | 37.65 | 35.74 | 5.09 | 5.59 | 10.25 | 2.70 | 1.72 | - | 1.25 |

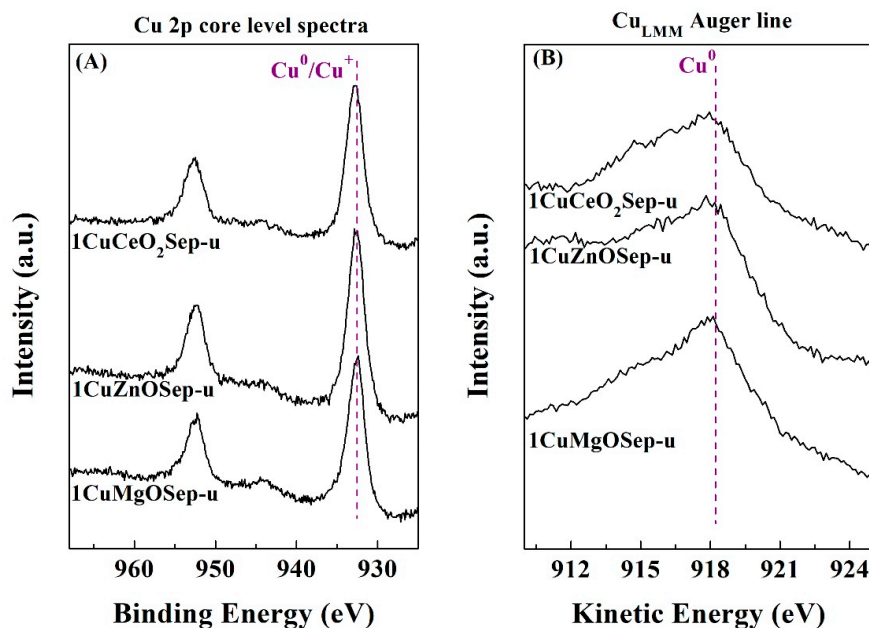


Figure 10. Cu 2p core level spectra (A) and Cu_{LMM} Auger line (B) of the Cu-based catalysts with oxide species and supported on sepiolite (Cu/M molar ratio of 1).

4. Materials and Methods

4.1. Materials

The clay mineral chosen to be used as support was a Mg-rich fibrous phyllosilicate as sepiolite, which was collected from Vicálvaro-Vallecas deposits (Spain), being commercialized by Tolsa S.A. as Pangel[®] S9. This product contains a purity greater than 95% with a small proportion of another Mg-rich smectites as stevensite. Sepiolite is a fibrous material, which contains ribbons with 2:1 type

layer structure, where each ribbon is linked to the next inverted SiO_4 tetrahedral sheet by Si–O bonds, leading to a fibrous framework with microcavities.

The copper precursor was copper nitrate trihydrate, $\text{Cu}(\text{NO}_3)_2 \cdot 3\text{H}_2\text{O}$ (99%, Sigma-Aldrich, St. Louis, MO, USA). The oxide species were incorporated from their respective nitrates, i.e., zinc nitrate tetrahydrate, $\text{Zn}(\text{NO}_3)_2 \cdot 4\text{H}_2\text{O}$ (99%, Merck, Darmstadt, Germany), magnesium nitrate hexahydrate, $\text{Mg}(\text{NO}_3)_2 \cdot 6\text{H}_2\text{O}$ (99.9%, Aldrich, St. Louis, MO, USA) and cerium nitrate trihydrate, $\text{Ce}(\text{NO}_3)_4 \cdot 3\text{H}_2\text{O}$ (99%, Aldrich, St. Louis, MO, USA). These salts were dissolved using several solvents as H_2O Milli-Q® (Merck, Darmstadt, Germany), ethanol, $\text{CH}_3\text{CH}_2\text{OH}$ (95% vol., Prolabo, Radnor, PA, USA), ethylene glycol, $\text{C}_2\text{H}_6\text{O}_2$, (99%, Sigma-Aldrich, St. Louis, MO, USA), while sodium carbonate, Na_2CO_3 (99%, Sigma-Aldrich, St. Louis, MO, USA) was employed as precipitating agent.

Other chemicals employed in the catalytic study were: furfural (99%, Sigma-Aldrich, St. Louis, MO, USA), cyclopentyl methyl ether (CPME) (99.9%, Sigma-Aldrich, St. Louis, MO, USA) as solvent, and o-xylene (99.9%, Sigma-Aldrich, St. Louis, MO, USA) as internal standard, while the gases used were He (99.99%, Air Liquide, Paris, France), H_2 (99.999%, Air Liquide, Paris, France), N_2 (99.9999%, Air Liquide, Paris, France), H_2/Ar (99.99%, 10 vol.% in H_2 , Air Liquide, Paris, France), and $\text{N}_2\text{O}/\text{He}$ (99.99%, 5 vol.% in N_2O , Air Liquide, Paris, France).

4.2. Catalysts Preparation

Cu-based catalysts were synthesized by a precipitation–deposition method. In the case of the Cu-based catalyst supported on sepiolite, 1 g of sepiolite was dispersed in 75 mL of distilled water for 30 min, under stirring. Later, it was added a solution formed by 10 mL H_2O , 20 mL ethyleneglycol, 50 mL ethanol and the appropriate proportion of $\text{Cu}(\text{NO}_3)_2 \cdot 3\text{H}_2\text{O}$ to achieve a Cu content of 15 wt.%, a metallic loading with which a suitable catalytic performance was attained in previous studies. The suspension was heated at 80 °C and then, Cu species were precipitated by adding an aqueous solution of Na_2CO_3 (0.5 M) until reaching a pH of 11. After precipitation, the suspension was cooled at room temperature and aged for 24 h. Finally, the solid was filtered and dried at 90 °C for 12 h, and subsequently calcined at 400 °C for 2 h. The obtained catalyst was denoted as (CuSep).

For the catalysts where ZnO, MgO, or CeO_2 were also incorporated into the catalytic system, the corresponding nitrates were added to the sepiolite dispersion at the same time as copper nitrate. The synthetic procedure was similar to that previously described for CuSep. Three different Cu/M molar ratios were employed in the initial solution ($x = 0.4, 1$, and 2.5) for each basic or amphoteric oxide ($M = \text{Mg}$, Zn , and Ce), and samples were labeled as $x\text{CuMgOSep}$, $x\text{CuZnOSep}$, and $x\text{CuCeO}_2\text{Sep}$, while the Cu content (in wt.%) are compiled in Table 7. These catalysts were compared with the corresponding copper catalysts supported on these metal oxides (MgO , ZnO , and CeO_2) (Cu/M molar ratio of 1) without sepiolite, studied in previous research [22,31,34].

Table 7. Cu content (in wt.%) of the Cu-based catalysts with oxide species and supported on sepiolite.

| Catalyst | Cu Content (wt.%) |
|---------------------------|-------------------|
| CuSep | 15.0 |
| 0.4CuMgOSep | 10.8 |
| 1CuMgOSep | 12.0 |
| 2.5CuMgOSep | 12.6 |
| 0.4CuZnOSep | 9.2 |
| 1CuZnOSep | 11.2 |
| 2.5CuZnOSep | 12.2 |
| 0.4CuCeO ₂ Sep | 6.9 |
| 1CuCeO ₂ Sep | 9.6 |
| 2.5CuCeO ₂ Sep | 11.4 |

The obtained samples were labeled as 1CuMgO, 1CuZnO, and 1CuCeO₂. In all cases, the obtained precursors were reduced under H₂-flow (60 mL min^{−1}) from rt to 300 °C, maintaining this temperature during 1 h, according to their respective H₂-TPR profile.

4.3. Catalysts' Characterization

The H₂-TPR study was performed by using 0.08 g of catalyst precursor, which was previously treated at 100 °C during 45 min using a He-flow (35 mL min^{−1}). After the precursor was cooled at 50 °C, the H₂ consumption associated to reduction processes was registered in situ from 50 to 500 °C in an Ar/H₂-flow (10 vol.% of H₂), using a flow of 48 mL min^{−1} and a ramp of 10 °C min^{−1}. The H₂O generated along the reduction step was retained in a cold finger immersed in a i-propyl alcohol/liquid N₂ bath at about −80 °C. The H₂-consumption was registered on-line with a thermal conductivity detector (TCD).

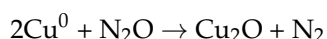
X-ray diffraction patterns were registered in a diffractometer (PANanalytical X'Pert Pro, Royston, UK). The powder samples were obtained in a Bragg-Brentano reflection configuration, using a Ge (111) monochromator, with a Cu Kα₁ radiation, and an X'Celerator detector (step size of 2θ: 0.017°). The size of the crystallites (D) was estimated from the Williamson–Hall equation, $B \cos(\theta) = (K\lambda/D) + (2\varepsilon \sin(\theta))$, where θ is the Bragg angle, B is the full width at half-maximum (FWHM) of the XRD peak, K is the Scherrer constant, λ is the X-ray wavelength, and ε is the lattice strain [43].

The morphology of the catalysts was determined by Transmission Electron Microscopy (TEM). The micrographs were performed using FEI Talos F200X equipment (Thermo Fisher Scientific, Waltham, MA, USA). This TEM equipment combines outstanding high-resolution TEM and S/TEM imaging with industry-leading energy dispersive X-ray spectroscopy (EDS) signal detection. The catalysts were suspended in 2-propanol and dropped onto a perforated carbon film grid.

The textural parameters of the samples were assessed from their N₂ adsorption-desorption isotherms at −196 °C using Micromeritics equipment (ASAP 2020, Norcross, GA, U.S.A). In a preliminary step, the samples were outgassed under vacuum (10^{−4} mbar) using a temperature of 200 °C during 12 h. The specific surface area was calculated from the BET equation, considering that the cross-section of the N₂ molecule is 16.2 Å² [49]. The pore volume was determined from the adsorption branch at P/P₀ = 0.996, while the pore width was estimated by the Density Functional Theory (DFT) method [45].

The quantification of the acid sites was performed by ammonia thermoprogrammed desorption (NH₃-TPD). In each analysis, 0.08 g of catalyst was treated under a He-flow (40 mL min^{−1}) from rt to 550 °C, using a heating ramp of 10 °C min^{−1}, and then was cooled to the reduction temperature. Later, the sample was treated with a H₂-flow of 60 mL min^{−1} for 1 h and cooled under a He-flow (40 mL min^{−1}) until 100 °C. After that, the catalyst was saturated with NH₃-flow for 5 min at this temperature. In the next step, a He-flow (40 mL min^{−1}) was passed to remove the NH₃-physisorbed. Finally, thermoprogrammed desorption was carried out by heating the samples from 100 to 550 °C, using a ramp of 10 °C min^{−1}. The NH₃-desorbed was quantified by a thermal conductivity detector (TCD).

The metallic surface and the dispersion of Cu⁰ species were determined by N₂O titration following the procedure described in previous research [31,34]. This methodology is based on the superficial oxidation of the Cu⁰ under a N₂O-flow, according to the reaction:



Prior the analysis, the catalytic precursor was reduced under a 10 vol.% H₂/Ar-flow (48 mL min^{−1}) at 300 °C for 1 h, with a heating rate of 5 °C min^{−1}. Later, catalysts (reduced samples) were cooled until 60 °C under a He flow. The Cu⁰-oxidation to Cu⁺ was performed by titration with N₂O (5 vol.% N₂O/He), at 60 °C for 1 h. Then, the sample was cleaned under an Ar-flow and cooled

to room temperature. Finally, the Cu₂O-reduction to Cu⁰ was carried out by heating from room temperature to 300 °C with a heating rate of 5 °C min^{−1}, being monitored its H₂-consumption by TCD.

The dispersion was determined from the H₂-TPR profiles as follows:

$$Dispersion = \frac{H_2 \text{ consumption } (Cu^+ \rightarrow Cu^0)}{H_2 \text{ consumption } (Cu^{2+} \rightarrow Cu^0)} \times 100$$

The metallic surface area was determined according to the methodology proposed by Pakharukova et al., by using the following equation [50]:

$$S_{Cu}^{N_2O} = \frac{M_{H_2} SF N_A}{10^4 C_M W_{Cu}}$$

where M_{H₂} is the amount of H₂ consumed per mass unit (μmol g^{−1}), SF is a stoichiometric factor (2), N_A is the Avogadro number, C_M is the number of copper atoms per surface area unit (1.46 × 10¹⁹ atoms m^{−2}), and W_{Cu} is the Cu content (wt.%).

Considering a spherical morphology of the Cu⁰ particles, the average size (nm) of the metallic particles was determined from:

$$d_{Cu}^{N_2O} = \frac{6 \times 10^3}{S_{Cu}^{N_2O} \rho_{Cu}}$$

where ρ is the density of copper (8.92 g cm^{−3}).

The chemical composition of samples on its surface was determined by X-ray photoelectron spectroscopy (XPS), using a spectrometer (Physical Electronics PHI 5700) with nonmonochromatic Mg Kα radiation (1253.6 eV, 300 W, 15 kV), and multichannel detector. Each spectrum was registered in the constant-pass energy mode at 29.35 eV with a diameter analysis area of 0.72 μm. The binding energy shift was corrected using the adventitious carbon (C 1s at binding energy = 284.8 eV) as reference. The acquisition and data analysis were performed using a software package (PHI ACCESS ESCA-V6.0F). In all cases, the signals were subtracted using a Shirley-type background and fitted with Gaussian–Lorentzian curves to determine more accurately the binding energies of the different element core levels. To avoid the oxidation of the catalysts, the samples were reduced ex-situ and then they were stored in sealed vials, to avoid its oxidation, with an inert solvent (cyclohexane). Samples were transferred to the XPS equipment in a dry box under a N₂-flow. Then, the solvent was removed by evaporation in a pre-chamber and the samples were introduced directly without previous treatment in the analytical chamber.

4.4. Catalytic Tests

The hydrogenation of FUR in the vapor phase was performed in a fixed-bed in a quartz tubular reactor with an internal diameter of a quarter of an inch (1/4") The pelletized sample (0.325–0.400 mm) was placed in the middle of the glass reactor between two layers of quartz wool. The temperature was controlled with a thermocouple, which is located at the same height of the catalytic bed. Prior of each test, the precursor was reduced in-situ using a H₂-flow of 60 mL min^{−1} at 300 °C for 1 h. Then, the catalyst was cooled until the selected reaction temperature was reached using the same H₂ flow (60 mL min^{−1}). The catalytic tests were performed using a flow (3.87 mL h^{−1}) of a FUR solution dissolved in CPME (5 vol.%) to reach a WHSV of 1.5 h^{−1}. This feed was pumped using a Gilson 307SC piston pump (model 10SC).

The reaction products were collected on an ice-finger. An aliquot of 1 mL was mixed with o-xylene, as internal standard and chloroform, to minimize problems associated to the solvent expansion in the injector of the GC. Then, this mixture was sealed in vials, being analyzed and quantified by gas chromatography, using a Shimadzu (GC-14A) apparatus, which is equipped with a flame ionization

detector (FID) and a capillary column (CP-Wax 52CB). The furfural conversion and selectivity were calculated and defined as follows:

$$\text{Conversion (\%)} = \frac{\text{mol of furfural converted}}{\text{mol of furfural fed}} \times 100$$

$$\text{Selectivity (\%)} = \frac{\text{mol of the product}}{\text{mol of furfural converted}} \times 100$$

5. Conclusions

A set of Cu⁰-based catalysts supported on an inexpensive clay mineral, sepiolite, has been synthesized and then assayed in FUR hydrogenation in vapor phase. The catalytic results reveal that the incorporation of basic and amphoteric metal oxides (MgO, ZnO, and CeO₂) into the catalytic system improves the catalytic activity as a consequence of the modification of the electronic density of metal Cu(0) particles. This fact favors the desorption of the FUR molecules and increases the availability of the active sites, as well as its resistance to deactivation.

Similar to other Cu-based catalysts, both FOL and MF are the only obtained products. In the present research, the main product is FOL. The MF content is directly related to the acidity of the catalytic system. Thus, the 1CuZnOsep catalyst displays the highest MF yield, although in all cases, this yield is lower than that reached for FOL.

The characterization of the catalysts reveals that the incorporation of these metal oxide species into the catalytic system decreases the Cu crystal size. This fact implies an increase of the available Cu sites, which is directly related to an improvement of the FUR conversion. In all cases, the catalysts are very stable in comparison to other catalytic systems reported in the literature. The progressive deactivation is ascribed to the formation of carbonaceous deposits, which block the Cu sites involved in the FUR hydrogenation. In this sense, the increase of the acid sites favors the formation of carbonaceous deposits, as was inferred from XPS data.

Author Contributions: Conceptualization, P.M.-T. and J.A.C. devised the elaboration of this review. Funding acquisition, P.M.-T. obtained the funds coming from the project CTQ2015-64226-C3-3-R to carry out the research. Investigation, C.P.J.-G. and A.G.-T. performed the experiments and collected the data. Data curation, C.G.-S., J.M.M.-R. and J.A.C. produced and scrubbed the data reported in this manuscript. Methodology, C.G.-S., P.M.-T., and J.A.C. developed the methodology of this research. Project administration, managed and coordinated C.G.-S., P.M.-T. and J.A.C. managed and coordinated the research. Supervision, P.M.-T., J.J.Q.-S. and J.A.C. planned the core of the present research. Writing—original draft, J.M.M.-R. and J.A.C. wrote the first draft of the present manuscript. Writing—review & editing, C.G.-S., P.M.-T. and J.A.C. revised and completed the first draft.

Funding: This research was funded by the Ministry of Economy and Competitiveness (Spain), grant numbers (CTQ2015-64226-C3-3-R, IEDI-2016-00743), Junta de Andalucía (Spain) (P12-RNM-1565), and FEDER (European Union) funds.

Acknowledgments: J.A.C. and C.G.-S. thank Malaga University for the financial support.

Conflicts of Interest: The authors declare no conflicts of interest.

References

1. Bozell, J.J.; Petersen, G.R. Technology development for the production of biobased products from biorefinery carbohydrates—The US Department of Energy's "Top 10" revisited. *Green Chem.* **2010**, *12*, 539–554. [[CrossRef](#)]
2. Mariscal, R.; Maireles-Torres, P.; Ojeda, M.; Sádaba, I.; Lopez-Granados, M. Furfural: A renewable and versatile platform molecule for the synthesis of chemicals and fuels. *Energy Environ. Sci.* **2016**, *9*, 1144–1189. [[CrossRef](#)]
3. Lange, J.P.; van der Heide, E.; van Buijtenen, J.; Price, R. Furfural—A promising platform for lignocellulosic biofuels. *ChemSusChem* **2012**, *5*, 150–166. [[CrossRef](#)] [[PubMed](#)]
4. Li, X.; Jia, P.; Wang, T. Furfural: A Promising Platform Compound for Sustainable Production of C₄ and C₅ Chemicals. *ACS Catal.* **2016**, *6*, 7621–7640. [[CrossRef](#)]

5. Gong, W.; Chen, C.; Zhang, Y.; Zhou, H.; Wang, H.; Zhang, H.; Zhang, Y.; Wang, G.; Zhao, H. Efficient synthesis of furfuryl alcohol from H₂-hydrogenation/transfer hydrogenation of furfural using sulfonate group modified Cu catalyst. *ACS Sustain. Chem. Eng.* **2017**, *5*, 2172–2180. [\[CrossRef\]](#)
6. Villaverde, M.M.; Garetto, T.F.; Marchi, A.J. Liquid-phase transfer hydrogenation of furfural to furfuryl alcohol on Cu-Mg-Al catalysts. *Catal. Commun.* **2015**, *58*, 6–10. [\[CrossRef\]](#)
7. Yuan, Q.; Zhang, D.; van Haandel, L.; Ye, F.; Xue, T.; Hensen, E.J.M.; Guan, Y. Selective liquid phase hydrogenation of furfural to furfuryl alcohol by Ru/Zr-MOFs. *J. Mol. Catal. A Chem.* **2015**, *406*, 58–64. [\[CrossRef\]](#)
8. Scotti, N.; Zaccheria, F.; Bisio, C.; Vittoni, C.; Ravasio, N. Switching selectivity in the hydrogen transfer reduction of furfural. *Chem. Select* **2018**, *3*, 8344–8348. [\[CrossRef\]](#)
9. Li, J.; Liu, J.L.; Zhou, H.J.; Fu, Y. Catalytic transfer hydrogenation of furfural to furfuryl alcohol over nitrogen-doped carbon-supported iron catalysts. *ChemSusChem* **2016**, *9*, 1339–1347. [\[CrossRef\]](#) [\[PubMed\]](#)
10. Kim, M.S.; Simanjuntak, F.S.H.; Lim, S.; Jae, J.; Ha, J.M.; Lee, H. Synthesis of alumina–carbon composite material for the catalytic conversion of furfural to furfuryl alcohol. *J. Ind. Eng. Chem.* **2017**, *52*, 59–65. [\[CrossRef\]](#)
11. López-Asensio, R.; Cecilia, J.A.; Jiménez-Gómez, C.P.; García-Sancho, C.; Moreno-Tost, R.; Maireles-Torres, P. Selective production of furfuryl alcohol from furfural by catalytic transfer hydrogenation over commercial aluminas. *Appl. Catal. A Gen.* **2018**, *556*, 1–9. [\[CrossRef\]](#)
12. López-Asensio, R.; Jiménez Gómez, C.P.; García Sancho, C.; Moreno-Tost, R.; Cecilia, J.A.; Maireles-Torres, P. Influence of structure-modifying agents in the synthesis of Zr-doped SBA-15 silica and their use as catalysts in the furfural hydrogenation to obtain high value-added products through the Meerwein-Ponndorf-Verley reduction. *Int. J. Mol. Sci.* **2019**, *20*, 828. [\[CrossRef\]](#)
13. Lazier, W. Process for Hydrogenating Furfural. U.S. Patent US2077422A, 20 April 1937.
14. Rao, R.; Dandekar, A.; Baker, R.T.K.; Vannice, M.A. Properties of copper chromite in hydrogenation reactions. *J. Catal.* **1997**, *171*, 406–419. [\[CrossRef\]](#)
15. Merlo, A.B.; Vetere, V.; Ruggera, J.F.; Casella, M.L. Bimetallic PtSn catalyst for the selective hydrogenation of furfural to furfuryl alcohol in liquid-phase. *Catal. Commun.* **2009**, *10*, 1665–1669. [\[CrossRef\]](#)
16. Sitthisa, S.; Sooknoi, T.; Ma, Y.; Balbuena, P.B.; Resasco, D.E. Kinetics and mechanism of hydrogenation of furfural on Cu/SiO₂ catalysts. *J. Catal.* **2011**, *277*, 1–13. [\[CrossRef\]](#)
17. Wei, S.; Cui, H.; Wang, J.; Zhuo, S.; Yi, W.; Wang, L.; Li, Z. Preparation and activity evaluation of NiMoB/γAl₂O₃ catalyst by liquid-phase furfural hydrogenation. *Particuology* **2011**, *9*, 69–74. [\[CrossRef\]](#)
18. Sharma, R.V.; Das, U.; Sammynaiken, R.; Dalai, A.K. Liquid phase chemo-selective catalytic hydrogenation of furfural to furfuryl alcohol. *Appl. Catal. A Gen.* **2013**, *454*, 127–136. [\[CrossRef\]](#)
19. Villaverde, M.M.; Bertero, N.M.; Garetto, T.F.; Marchi, A.J. Selective liquid-phase hydrogenation of furfural to furfuryl alcohol over Cu-based catalysts. *Catal. Today* **2013**, *213*, 87–92. [\[CrossRef\]](#)
20. Yan, K.; Jarvis, C.; Lafleur, T.; Qiao, Y.; Xie, X. Novel synthesis of Pd nanoparticles for hydrogenation of biomass-derived platform chemicals showing enhanced catalytic performance. *RSC Adv.* **2013**, *3*, 25865–25871. [\[CrossRef\]](#)
21. Sitthisa, S.; Resasco, D.E. Hydrodeoxygenation of furfural over supported metal catalysts: A comparative study of Cu, Pd, and Ni. *Catal. Lett.* **2011**, *141*, 784–791. [\[CrossRef\]](#)
22. Nagaraja, B.M.; Kumar, V.S.; Shasikala, V.; Padmasri, A.H.; Sreedhar, B.; Raju, B.D.; Rama Rao, K.S. A highly efficient Cu/MgO catalyst for vapour phase hydrogenation of furfural to furfuryl alcohol. *Catal. Commun.* **2003**, *4*, 287–293. [\[CrossRef\]](#)
23. Nagaraja, B.M.; Padmasri, A.H.; Raju, B.D.; Rama Rao, K.S. Vapor phase selective hydrogenation of furfural to furfuryl alcohol over Cu-MgO coprecipitated catalysts. *J. Mol. Catal. A Chem.* **2007**, *265*, 90–97. [\[CrossRef\]](#)
24. Yan, K.; Wu, G.; Lafleur, T.; Jarvis, C. Production, properties and catalytic hydrogenation of furfural to fuel additives and value-added chemicals. *Renew. Sustain. Energy Rev.* **2014**, *38*, 663–676. [\[CrossRef\]](#)
25. Dong, F.; Zhu, Y.; Zheng, H.; Zhu, Y.; Li, X.; Li, Y. Cr-free Cu-catalysts for the selective hydrogenation of biomass-derived furfural to 2-methylfuran: The synergistic effect of metal and acid sites. *J. Mol. Catal. A Chem.* **2015**, *398*, 140–148. [\[CrossRef\]](#)

26. Vargas-Hernández, D.; Rubio-Caballero, J.M.; Santamaría-González, J.; Moreno-Tost, R.; Merida-Robles, J.M.; Pérez-Cruz, M.A.; Jiménez-López, A.; Hernández-Huesca, R.; Maireles-Torres, P. Furfuryl alcohol from furfural hydrogenation over copper supported on SBA-15 silica catalysts. *J. Mol. Catal. A Chem.* **2014**, *383*, 106–113. [[CrossRef](#)]
27. Wu, J.; Shen, Y.; Liu, C.; Wang, H.; Geng, C.; Zhang, Z. Vapor phase hydrogenation of furfural to furfuryl alcohol over environmentally friendly Cu-Ca/SiO₂ catalyst. *Catal. Commun.* **2005**, *6*, 633–637. [[CrossRef](#)]
28. Manikandan, M.; Venugopal, A.K.; Nagpure, A.S.; Chilukuri, S.; Raja, T. Promotional effect of Fe on the performance of supported Cu catalyst for ambient pressure hydrogenation of furfural. *RSC Adv.* **2016**, *6*, 3888–3898. [[CrossRef](#)]
29. Ghashghaee, M.; Sadjadi, S.; Shirvani, S.; Farzaneh, V. A novel consecutive approach for the preparation of Cu–MgO catalysts with high activity for hydrogenation of furfural to furfuryl alcohol. *Catal. Lett.* **2017**, *147*, 318–327. [[CrossRef](#)]
30. Shirvani, S.; Ghashghaee, M.; Farzaneh, V.; Sadjadi, S. Influence of catalyst additives on vapor-phase hydrogenation of furfural to furfuryl alcohol on impregnated copper/magnesia. *Biomass Convers. Biorefin.* **2018**, *8*, 79–86. [[CrossRef](#)]
31. Jiménez-Gómez, C.P.; Cecilia, J.A.; Durán-Martín, D.; Moreno Tost, R.; Santamaría González, J.; Mérida Robles, J.M.; Mariscal, R.; Maireles-Torres, P. Gas-phase hydrogenation of furfural to furfuryl alcohol over Cu/ZnO catalysts. *J. Catal.* **2016**, *336*, 107–115. [[CrossRef](#)]
32. Yang, X.; Xiang, X.; Chen, H.; Zheng, H.; Li, Y.W.; Zhu, Y. Efficient synthesis of furfuryl alcohol and 2-methylfuran from furfural over mineral-derived Cu/ZnO catalysts. *ChemCatChem* **2017**, *9*, 3023–3030. [[CrossRef](#)]
33. Yang, X.; Chen, H.; Meng, Q.; Zheng, H.; Zhu, Y.; Li, Y.W. Insights into influence of nanoparticle size and metal–support interactions of Cu/ZnO catalysts on activity for furfural hydrogenation. *Catal. Sci. Technol.* **2017**, *7*, 5625–5634. [[CrossRef](#)]
34. Jiménez-Gómez, C.P.; Cecilia, J.A.; Márquez-Rodríguez, I.; Moreno-Tost, R.; Santamaría-González, J.; Mérida-Robles, J.M.; Maireles-Torres, P. Gas-phase hydrogenation of furfural over Cu/CeO₂ catalysts. *Catal. Today* **2017**, *279*, 327–338. [[CrossRef](#)]
35. Jiménez-Gómez, C.P.; Cecilia, J.A.; Moreno-Tost, R.; Maireles Torres, P. Selective furfural hydrogenation to furfuryl alcohol using Cu-based catalysts supported on clay minerals. *Top. Catal.* **2017**, *60*, 1040–1053. [[CrossRef](#)]
36. Shi, Y.; Zhu, Y.; Yang, Y.; Li, Y.W.; Jiao, H. Exploring furfural catalytic conversion on Cu(111) from computation. *ACS Catal.* **2015**, *5*, 4020–4032. [[CrossRef](#)]
37. Jiménez-Gómez, C.P.; Cecilia, J.A.; Moreno-Tost, R.; Maireles-Torres, P. Selective production of 2-methylfuran by gas-phase hydrogenation of furfural on copper incorporated by complexation in mesoporous silica catalysts. *ChemSusChem* **2017**, *10*, 1448–1459. [[CrossRef](#)] [[PubMed](#)]
38. Liu, D.; Zemlyanov, D.; Wu, T.; Lobo-Lapidus, R.J.; Dumesic, J.A.; Miller, J.T.; Marshall, C.L. Deactivation mechanistic studies of copper chromite catalyst for selective hydrogenation of 2-furfuraldehyde. *J. Catal.* **2013**, *299*, 336–345. [[CrossRef](#)]
39. Cecilia, J.A.; Arango-Díaz, A.; Marrero-Jerez, J.; Núñez, P.; Moretti, E.; Storaro, L.; Rodríguez-Castellón, E. Catalytic behaviour of CuO–CeO₂ systems prepared by different synthetic methodologies in the CO-PROX reaction under CO₂–H₂O feed stream. *Catalysts* **2017**, *7*, 160. [[CrossRef](#)]
40. Gamarra, D.; Hornés, A.; Koppány, Z.; Schay, Z.; Munuera, G.; Soria, J.; Martínez-Arias, A. Catalytic processes during preferential oxidation of CO in H₂-rich streams over catalysts based on copper-ceria. *J. Power Sources* **2007**, *169*, 110–116. [[CrossRef](#)]
41. Franco, F.; Pozo, M.; Cecilia, J.A.; Benítez-Guerrero, M.; Pozo, E.; Martín Rubí, J.A. Microwave assisted acid treatment of sepiolite: The role of composition and “crystallinity”. *Appl. Clay Sci.* **2014**, *102*, 15–27. [[CrossRef](#)]
42. Cecilia, J.A.; Vilarrasa-García, E.; Cavalcante, C.L., Jr.; Azevedo, D.C.S.; Franco, F.; Rodríguez-Castellón, E. Evaluation of two fibrous clay minerals (sepiolite and palygorskite) for CO₂ Capture. *J. Environ. Chem. Eng.* **2018**, *6*, 4573–4587. [[CrossRef](#)]
43. Williamson, G.K.; Hall, W.H. X-ray broadening from fcc aluminium and wolfram. *Acta Metall.* **1953**, *1*, 22–31. [[CrossRef](#)]

44. Thommes, M.; Kaneko, K.; Neimark, A.V.; Oliver, J.P.; Rodríguez-Reinoso, F.; Rouquerol, J.; Sing, K.S.W. Physisorption of gases, with special reference to the evaluation of surface area and pore size distribution (IUPAC technical report). *Pure Appl. Chem.* **2015**, *87*, 1051–1069. [\[CrossRef\]](#)
45. Landers, J.; Gor, G.; Neimark, A. Density functional theory methods for characterization of porous materials. *Colloids Surf. A Physicochem. Eng. Asp.* **2013**, *437*, 3–32. [\[CrossRef\]](#)
46. Suárez, M.; García-Romero, E. Advances in the crystal chemistry of sepiolite and palygorskite. *Dev. Clay Sci.* **2011**, *3*, 33–65.
47. Scotti, N.; Dangate, M.; Gervasini, A.; Evangelisti, C.; Ravasio, N.; Zaccheria, F. Unraveling the role of low coordination sites in a Cu metal nanoparticle: A step toward the selective synthesis of second generation biofuels. *ACS Catal.* **2014**, *4*, 2818–2826. [\[CrossRef\]](#)
48. Moulder, J.F.; Stickle, W.F.; Sool, P.E.; Bombier, K.D. *Handbook of X-ray Photoelectron Spectroscopy*; Pekin-Elmer: Eden Prairie, NM, USA, 1992.
49. Brunauer, S.; Emmett, P.; Teller, E. Adsorption of gases in multimolecular layers. *J. Am. Chem. Soc.* **1938**, *60*, 309–319. [\[CrossRef\]](#)
50. Pakharukova, V.P.; Moroz, E.M.; Zyuzin, D.A.; Ishchenko, A.V.; Dolgikh, L.Y.; Strizhak, P.E. Structure of copper oxide species supported on monoclinic zirconia. *J. Phys. Chem. C* **2015**, *119*, 28828–28835. [\[CrossRef\]](#)



© 2019 by the authors. Licensee MDPI, Basel, Switzerland. This article is an open access article distributed under the terms and conditions of the Creative Commons Attribution (CC BY) license (<http://creativecommons.org/licenses/by/4.0/>).